Journal of Hydrology: Regional Studies 44 (2022) 101209

Contents lists available at ScienceDirect

Journal of Hydrology: Regional Studies

journal homepage: www.elsevier.com/locate/ejrh

The effect of afforestation on moist heat stress in Loess Plateau, China

Shulin Zhang [a,b,c,d], Weiguang Wang [a,b,c], Adriaan J. Teuling [d,*], Guoshuai Liu [a,b,c], Olusola O. Ayantobo [e], Jianyu Fu [a,b,c], Qing Dong [a,b,c]

[a] State Key Laboratory of Hydrology-Water Resources and Hydraulic Engineering, Hohai University, Nanjing 210098, China
[b] Key Laboratory of Water Big Data Technology of Ministry of Water Resources, Hohai University, Nanjing 210098, China
[c] College of Water Resources and Hydrology, Hohai University, Nanjing 210098, China
[d] Hydrology and Quantitative Water Management Group, Wageningen University & Research, Wageningen, the Netherlands
[e] State Key Laboratory of Hydroscience and Engineering, Department of Hydraulic Engineering, Tsinghua University, Beijing 10086, China

ARTICLE INFO

Keywords:
Afforestation
Moist heat stress
Climate change
Heat fluxes
Loess Plateau

ABSTRACT

Study region: Loess Plateau (LP), China

Study focus: This study aimed to research whether and to what degree afforestation contributes to the variations in moist heat stress in the study area. Here, wet bulb, temperature (*Tw*) was used to quantify the moist heat stress. Subsequently, The Weather Research and Forecasting model (WRF) is applied to simulate the modulation of climate change related to afforestation during 2001–2015. Based on the analysis of energy fluxes, we identified the biogeophysical mechanism of afforestation impact on moist heat stress.

New hydrological insights for the region: Since the operation of the "Grain-to-Green" program, LP has experienced widespread afforestation which perturbs energy and water fluxes, affecting regional climate regimes. The forest expansion increases relative humidity but cools the regional temperature. As a significant combined climate factor, the average moist heat stress decreases with the magnitude of $-0.1\sim-0.3$ °C in central LP. While the decrease rate of *Tw* is slower than near-surface temperature. It is worth noting that, an increased signal occurs in the maximum *Tw* (almost 0.2 °C in eastern and northeastern LP), which might expose humans to the risk of moist heat stress. By the mechanistic analysis, the research shows that the near-surface temperature and sensible heat flux are dominant driving factors for the change of *Tw*. Furthermore, the subsidence of the planetary boundary layer enhances moist heat stress. Overall, afforestation's effects on land surface-atmosphere interaction are non-negligible and the moist heat stress should be accounted for in climate change adaptation strategies.

1. Introduction

Global warming is an undeniable reality (Kerr, 2007; Xu et al., 2018), and most research on heat stress extremes under continued warming tends to focus on independent climate indicators such as temperature, precipitation, etc. (Cao et al., 2019; Zhang and Liang, 2018). However, some researches investigate that heat stress extremes were more frequently associated with surface humidity

* Corresponding author.
E-mail address: ryan.teuling@wur.nl (A.J. Teuling).

https://doi.org/10.1016/j.ejrh.2022.101209
Received 31 May 2022; Received in revised form 30 August 2022; Accepted 11 September 2022
Available online 16 September 2022

variation than surface temperature variation (Raymond et al., 2017, Sherwood, 2018, Kang and Eltahir, 2018), so it is not convinced to research heat stress using a single indicator, that is to say, the heat stress is moderated by moisture (Mishra et al., 2020). As one of the most severe heat hazards, moist heat stress greatly challenges economic activities, agricultural resources, and ecosystems, significantly affecting human health. It is well-established that due to extreme heat stress events, there is a substantial reduction in work productivity (Zander et al., 2015; Kjellstrom et al., 2016; Rao et al., 2020). Moreover, moist heat stress will decrease the body's evaporation rate and exacerbate physiological heat stress, increasing morbidity and mortality (Raymond et al., 2017, Freychet et al., 2020). In China, some areas have already witnessed moist heat stress conditions during summer from 1971 to 2014 (Luo and Lau, 2021; Freychet et al., 2020), meaning that more people will be exposed to heat stroke. However, most of the research ignored the interaction between landcover and the atmosphere, leading to more uncertainty in researching the impact of moist heat stress. There is still no clear consensus about how moist heat stress-related risks emerge from the interplay between natural heat acclimatization and human activity.

Nowadays, studying the mechanism of human activity in the land-atmosphere process is attracting increasing attention. Intensive anthropogenic activities (e.g., urbanization, land cover change, irrigation, etc.) modifies land-atmosphere processes through the alteration of the regional water cycle and energy transfer (Cherubini et al., 2018), which in turn affects the region's micro-climate. Many researchers have investigated the impact of irrigation and urbanization on moisture content (Mishra et al., 2020, Yang et al., 2021). However, as one of the essential human-mediated activities, afforestation has a visible effect on the regional moisture heat stress. The revegetation influences the climate not only by the biogeochemical process (carbon sequestration) (Forzieri et al., 2017) but also by biogeophysical processes (Davin and Noblet-Ducoudré, 2010). The greening trend changes biogeophysical characteristics, affecting energy and water fluxes (Keenan et al., 2016). On the one hand, open terrain has a higher albedo than forest (Betts, 2000; Betts, 2011; Jach et al., 2020), so more radiation is absorbed after forest expansion, which leads to an increase in available energy, hence to warming (Gibbard et al., 2005; Bonan et al., 2008; Lansu et al., 2020). On the other hand, afforestation creates a deeper root system and greater transpiring leaf area, which will promote latent heat flux and cool the surface (Peng et al., 2014, Bright et al., 2015). As a result, the balance of radiation and heat flux impacts determines which mechanism has the greater influence on regional climate. Scholars have made numerous attempts to demonstrate that afforestation modifies the occurrence of climate factors (including precipitation, evapotranspiration patterns) (Hoek van Dijke et al., 2022; Odoulami et al., 2019; Teuling et al., 2019; Hu et al., 2019; Abiodun et al., 2013; Teuling et al., 2010; Zhang et al., 2019). Many of these are studies on temperature. Due to the different in biogeophysical processes, the impact of afforestation on temperature will vary from region to region. In tropical region, the dominant factor affecting the temperature is nonradiative forcing. Caused by the high rates of evapotranspiration in tropical forests, the temperature will decrease after afforestation (Betts, 2000; Li et al., 2015). As for boreal forests, afforestation lower albedo than before, warming the climate (Baldocchi et al., 2004). While there is still no clear consensus about whether the climate response of the temperate forest will be cooling or warming (Bonan et al., 2008). Moreover, the effect of afforestation on moisture heat stress is still unclear. Hence, modeling the impact of afforestation on temperature, humidity and moist heat stress with greater spatial-temporal details from energy balance is needed to explore how the change affects the local climate (Sylla et al., 2016).

China is one of the countries with the highest amounts of afforestation. As Remote sensing image shows, an extensive trend of revegetation has been observed in China (Zhai et al., 2015; Feng et al., 2013), with a greening area of 212 million ha in 2008 (Feng et al., 2016; *CFS, 2019*), especially in the Loess Plateau (LP). In 1999 the Chinese government established the "Grain to Green" (GTG) program (Cao et al., 2018; Han et al., 2021). Up to 2012, the extension of forest area in the central LP (Ningxia, Shanxi, and Shaanxi) accounted for 11.2 % of the land area of the three provinces (Xiao, 2014). To quantify the afforestation influence on climate, previous studies have demonstrated the change of single climate factors related to afforestation, such as temperature, precipitation, etc. (Cao et al., 2019). However, the cumulative effects of afforestation continue to directly impact ecosystem functions due to other factors such as moist heat stress, which are crucial yet uncertain in LP. With the dual influence of global warming and afforestation, exposure to the risk of high moist heat stress will cause a severe impact on the local economy, human living comfort, and agricultural production (Koteswara et al., 2020). Meanwhile, given that LP has a population of more than 0.1 billion people (data from the '*Outline of Comprehensive Management Planning for the Loess Plateau (2010–2030)*'), clearing how climate change and large-scale afforestation affect local moist heat stress is a critical scientific topic with practical implications. Therefore, it is essential to detect whether and to what degree afforestation contributes to the moisture heat condition (Huang et al., 2020) after implementing the 'GTG' program in the LP.

Afforestation and its climatic implications on a regional scale have been investigated with the ultimate goal of statistically defining the climate response, particularly the moist heat response to land surface change. In general, the methodologies can be divided into empirical studies (based on observed data, such as in situ observation and satellite observations) (Zhang et al., 2014; Zhang and Liang, 2018) and Land-atmosphere interactions model simulations (Lansu et al., 2020; Jach et al., 2020; Li et al., 2016; Alkama and Cescatti, 2016; van Heerwaarden and Teuling, 2014). In most cases, the latter effectively isolates land cover change's radiative and nonradiative processes. Thus, modeling tools are pretty helpful in determining how vital vegetation greening can be in moderating climate changes worldwide (Ge et al., 2019). To study the impact of afforestation on the land surface-atmosphere interaction, we used the Weather Research and Forecasting model (WRF) and generated control and vegetation greening scenarios. We investigated the association between moist heat stress and the elements that contribute to it. Our goal was to (1) assess the magnitudes of vegetation change in LP during the summer (June, July, and August) from 2001 to 2015; (2) analyze the climate response to different greening scenarios, and (3) investigate the impact of afforestation on energy flux to determine the biogeophysical mechanisms of afforestation's climatic effect.

2. Study area

The Loess Plateau, one of the most extensive plateaus in China, is located between 104°54′ E~114°33′ E and 33°43′ N~41°16′ N, covering an area of about 620,000 km^2. The altitude is approximately 800–3000 m. Influenced by the East Asian and South Asian summer monsoon activity (Liu et al., 2016, Shi et al., 2020), the climate of LP is characterized by wet and warm in summer and dry and cold in winter. LP is an arid and semi-arid area (Kong et al., 2020), with the average annual precipitation and temperature varying from 110 mm to 860 mm and 4–14 °C, respectively. The LP is mainly covered with highly erodible loess layers with surface thickness ranging from 50 to 80 m. As one of the world's most severe soil erosion areas (Chen et al., 2007), soil erosion in LP is 4.54 million km^2, accounting for 71.5% of the total area. The erosion modulus is approximately 4000 t/km^2. The ecological environment in LP has been seriously damaged due to water resource shortage, desertification, soil erosion, and overgrazing. With the goal of ecosystem restoration, ensuring the safety of the ecological environment, and achieving more sustainable environmental conditions, the Chinese government launched the 'Grain to Green program' in 1999 (Cao et al., 2019). In LP, natural vegetation types vary from broad-leaved deciduous forest to steppe and then to arid desert in the direction from southeast to northwest (Wu et al., 2019). After 'GTG' program, many areas of crops converted to forest land and grassland (Hu et al., 2021). As statistic data shows that afforestation areas in the LP account for approximately 40 % of afforest areas in China (Office of the National Greening Committee, 2019). From 2001–2016, the area of forest net gain was 48, 786 km^2, and the percentage of the forested area increased from 8.19 % to 15.82 % approximate (Wang et al., 2018). The NDVI followed a significant upward trend with annual change rates of 0.15 % during 1985–2015 (Qu et al., 2020).

3. Material and methods

3.1. Materials

The leaf area index (LAI), vegetation fraction (FVC), albedo, and land cover data are updated to characterize the change in vegetation cover. The LAI and albedo are obtained from the Global Land Surface Satellite (GLASS) dataset (http://gre.geodata.cn/thematicView/GLASS.html) (Liang et al., 2013). The LAI and albedo are developed from an 8-day-average data at 0.05°× 0.05°

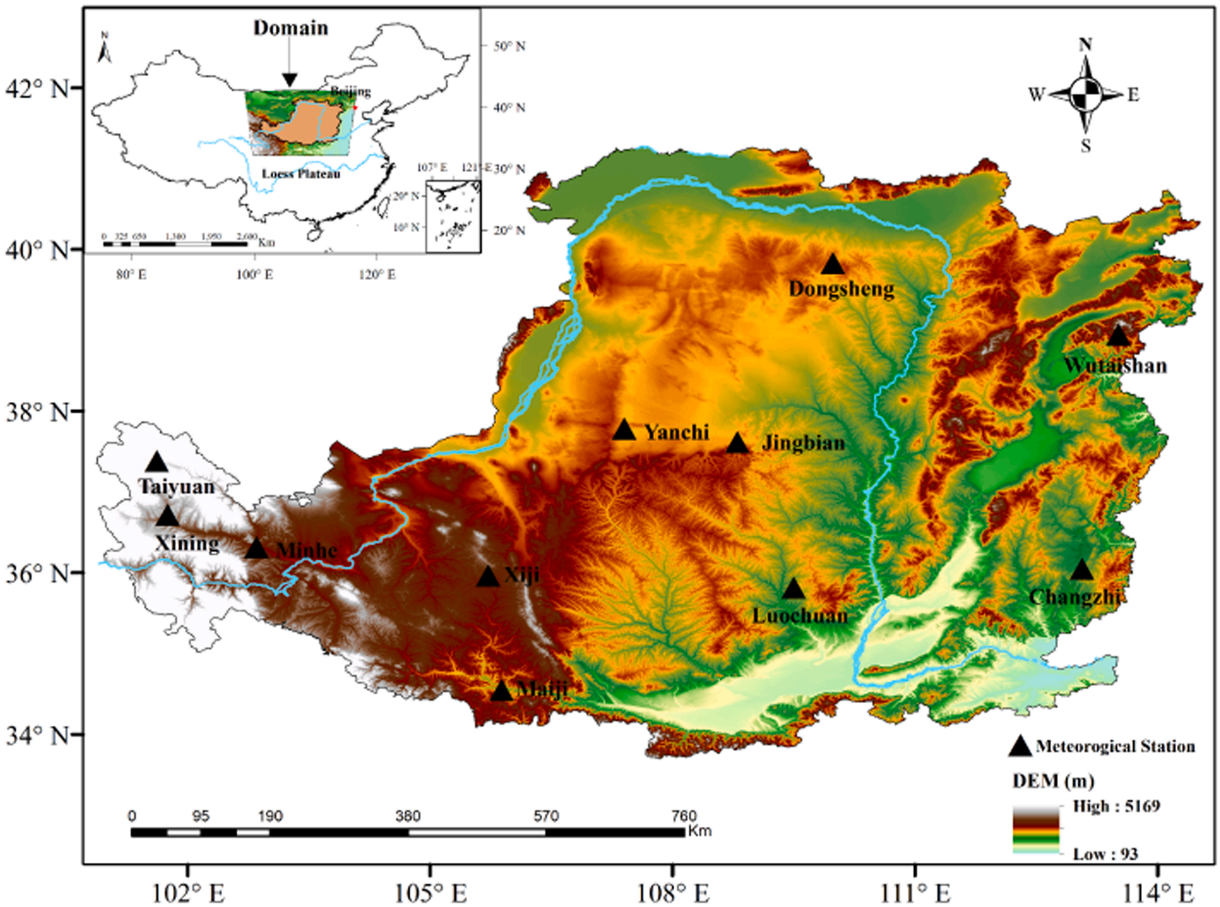

Fig. 1. Digital Elevation Map (DEM) and location of the 11 surface meteorologic stations in LP.

resolution on a grid from 1982 to 2018. The albedo provides both black-sky albedo and white-sky albedo, and the overall surface albedo is derived from the average black-sky albedo and white-sky albedo (Su et al., 2007*)*. According to Beer's law (Norman et al., 1995), the FVC is associated with LAI. To match the input data pattern of WRF, the 8-day-average data of LAI, FVC, and albedo are averaged into monthly data between 2001 and 2015. The land cover is satellite observation derived from a Moderate Resolution Imaging Spectroradiometer (MODIS). According to the principle of "International Geosphere-Biosphere Program" (IGBP) classification scheme, the land cover data are separated into 17 vegetation types at a resolution of $0.05^{\circ} \times 0.05^{\circ}$, including 11 categories of natural vegetation, three classes of mosaic types, and three classes of nonvegetative lands (Friedl et al., 2002).

Many reanalysis products can be utilized to force WRF. However, reanalysis datasets have different deficiencies on various temporal-spatial scales. As previous researches suggested that the ERA-interim shows a better agreement with Chinese separate stations (Zhu et al., 2017) for precipitation, temperature, and soil moisture, (Decker et al., 2012*;* Deng et al., 2020). Therefore, the initial and lateral boundary conditions for WRF are obtained from European Centre for Medium-Range Weather Forecasts (ECMWF) through ERA-Interim reanalysis data (https://www.Ecmwf.int/en/forecasts/datasets/reanalysis-datasets/era-interim) (Dee et al., 2011). It is the data with a 6-hr temporal resolution and a 0.5° spatial resolution since 1979. Benefiting from the developments of the ECMWF integrated forecasting system, the ERA-Interim dataset improved lots of parameterizations in the land surface scheme compared to the original data (Balsamo et al., 2015). The dataset has been widely used due to a variational bias correction technique and directly assimilated into early satellite radiance data. Therefore, it is an excellent dataset for climate studies (Jiang et al., 2011*,* Liu et al., 2018).

To evaluate the performance of the WRF model, we obtain observed data from the National Surface Weather Data Day Value Dataset (V3.0), produced by China Meteorological Data Service Center (http://data.cma.cn/data/cdcindex/cid/6d1b5efbdcbf9a58.html). This dataset includes the daily near-surface air temperature, surface air pressure, and surface air specific humidity from 699 Chinese meteorological stations. The dataset was proved reliable and used widely (Wu et al., 2020*;* Xiao et al., 2018). 11 uniform distributed station data were chosen for this topic in LP (Fig. 1).

3.2. WRF simulation

Many studies have used WRF to simulate the climate, e.g., precipitation (Knist et al., 2020*;* Cardoso et al., 2013*;* Srinivas et al., 2013) and temperature (Chotamonsak et al., 2011). Meanwhile, it is feasible to research the impact of land cover change on the climate through WRF (Chen et al., 2017; Yu et al., 2020a) and provides multi-physics to adapt the research area (Stegehuis et al., 2015). In this study, the effects of land cover change on regional climate were simulated using WRF/ARW (V4.2.0) in a one-way nested model with a horizontal domain of 20 km × 20 km (74 ×58 horizontal cells) and 37 vertical sigma layers. The center was located at 37.50°N, 107.5°E. The relevant physics parameterizations of the simulation are included in Table 1. WSM 3-class simple ice scheme was chosen as a microphysics option. The RRTMG scheme was turned on to be more suitable for long and shortwave radiation options. In order to improve the accuracy of the simulation, the Multi-scale Kain-Fritsch scheme was chosen as the cumulus option, YSU scheme was selected as the boundary-layer option, and the revised MM5 Monin-Obukhov scheme was chosen as the surface-layer option. The Noah land surface model (Noah-LSM), coupled with WRF, was utilized to simulate the energy variation or water cycle process between land and atmosphere (Cao et al., 2019). In the Noah-LSM, the default physical parameters of LAI, FVC, and albedo are the functions of the land-use category. They can be calculated through their maximum and minimum provided by the VEGPARM.TBL in WRF. The physical parameters cannot represent the natural land surface condition. To assess the feedback of different land cover on climate, we modified the default land use type into two simulation scenarios (in Section 3.2) based on MODIS data, which accurately described the different land cover types and their changes. The default vegetation parameters (LAI, FVC, and albedo) were replaced with GLASS dataset to ensure that the simulation results were closer to the actual situation.

3.3. Simulation scenario

To explore the process of land-atmosphere feedback in LP, we performed two sets of simulations. One considered vegetation greening scenario (VGS), in which the land cover classifications, LAI, FVC, and albedo in 2015 were used to approximate the current surface biogeophysical status. One was a control scenario (CTL), which considered a no-vegetation greening scenario with 2001 vegetation characteristics. WRF model simulated both scenarios with the same initial atmosphere conditions but different land cover biogeophysical parameters from 2000 to 2015 (The year 2000 was used to spin up the model). The simulations were in June, July, and August, and the choice was rooted in the perception that vegetation flourished in summer, hence a more vital interaction with the land atmosphere. Since both experiments' initial atmosphere and lateral boundary conditions do not vary, the climate differences between

Table 1
The main parameterizations scheme for WRF simulation.

Version	WRF/ARW (V4.2.0)
Horizontal resolution	20 km × 20 km
Microphysics option	The WRF Single-Moment 3 class microphysics scheme (WSM-3)
Radiation scheme	A new version of the Rapid Radiative Transfer Model (RRTM).
Cumulus	Multi-scale Kain-Fritsch
Planetary boundary-layer	The Yonsei University planetary boundary layer (PBL) scheme (YSU)
Surface-layer	The revised MM5 Monin-Obukhov scheme (MM5 similarity)

VGS and CTL will be attributed to land cover change.

3.4. Wet-bulb temperature

With the higher ambient air, the thermoregulation of the human body can be achieved by evaporation. However, the ability to keep temperature balance is limited by the humidity. Therefore, robust predictions of moist heat stress should consider humidity alongside temperature. Given that *Tw* stands out for its easy calculation and is more sensitive to humidity than other heat stress metrics (Sherwood, 2018), it was introduced in this research. *Tw* is a nonlinear relationship of near surface temperature and air humidity, (Ning et al., 2022; Safieddine et al., 2022) and a combined metric to measure mugginess (Davis et al., 2016; Raymond et al., 2017; Freychet et al., 2020), which was defined as a temperature that the air parcel would attain if cooled at constant pressure by evaporating water within it until saturation (Pal and Eltahir, 2016, Yao, 2022). The higher values of *Tw* the hotter and wetter conditions we will live, and vice versa (Yao et al., 2022). Heat episodes with high wet-bulb temperature can be dangerous to a human's health and lower the productivity of outdoor laborers. Therefore, it is preferable to quantify *Tw* affected by afforestation. It can be calculated from *T*, *p*, and humidity (Davies-Jones, 2008; Dunne et al., 2013):

$$E_s = 0.6108 \times \exp((17.27 \times (T - 273.15)/T)) \tag{1}$$

$$Ws = 621.97 \times E_s/(p - E_s) \tag{2}$$

$$W = rh/100 \times Ws \tag{3}$$

$$T_L = 1/((T - 55) - \ln(rh/100)/1840) + 55 \tag{4}$$

$$\theta_E = T \times (1000/p)^{(0.2854\times(1-0.28\times10^{-3}\times W))} \times \exp((3.376/(T_L - 0.00254)) \times W \times \left(1 + 0.81 \times 10^{-3} \times W\right) \tag{5}$$

$$T_W = 45.114 - 51.489 \times (\theta_E/273.15)^{-3.504} \tag{6}$$

Where T_W is the wet-bulb temperature (°C), it was designed to measure moist heat stress. E_s is the saturation vapor pressure (mbar) referenced from FAO56. *T* is the near-surface air temperature in Kelvins (K). *p* is the surface pressure (mbar) used to describe the saturation mixing ratio, *Ws* (g/kg). *rh* is the surface relative humidity. *W* is the mixing ratio (g/kg), T_L is the lifting condensation temperature (K). and θ_E is the equivalent potential temperature (K).

3.5. Model evaluation

To better compare the simulation with the observed climate, the output data of WRF were interpolated to the sites. Then the statistical indicators, including bias and correlation coefficient (R), were applied to evaluate the model performances across 11 stations in 2001 (Zheng et al., 2020). Due to the errors in input data and intrinsic limitations of the model, some inevitable biases occur in the simulation. Table 2 shows that the temperature and absolute percent simulation bias was − 0.96–1.43 °C and 4.9~12.0 %, respectively. The relative humidity and absolute percent simulation bias was − 17.86 %~11.42 % and 0.4~17.8 %, respectively. The simulations were generally highly correlated in a daily resolution with the observation, with the average R= 0.98 (P < 0.01, *F*-test) and R= 0.64 (P < 0.01, *F*-test) for surface temperature and relative humidity, respectively. Thus, it is acceptable to use the model to simulate climate behaviors.

Table 2
Bias and correlation coefficient between daily simulation and observation data in 2001 across LP.

Sitename	Lat	Lon	Surface temperature			Relative humidity		
			Bias (°C)	|Percent bias (%)|	R	Bias (%)	|Percent bias (%)|	R
Taiyuan	37.38	101.62	1.43	6.7	0.97	0.85	0.4	0.74
Xining	36.72	101.75	-0.59	11.8	0.98	11.42	11.3	0.72
Minhe	36.32	102.85	-0.54	9.8	0.98	5.46	9.3	0.65
Wutaishan	38.95	113.52	-0.96	10.9	0.98	-8.42	17.8	0.71
Yanchi	37.78	107.40	-0.35	11.7	0.98	-13.87	13.0	0.55
Jingbian	37.62	108.80	0.29	10.3	0.98	-14.65	13.6	0.59
Changzhi	36.05	113.07	-0.46	4.9	0.98	1.13	1.9	0.63
Xiji	35.97	105.72	-0.54	12.0	0.98	-7.40	12.7	0.68
Luochuan	35.82	109.50	-0.17	7.7	0.98	-5.65	14.6	0.66
Maiji	34.55	105.88	0.50	8.0	0.97	0.16	9.5	0.55
Dongsheng	39.83	109.98	1.39	5.2	0.98	-17.86	15.1	0.55

Notes: the |percent bias| represents the absolute value of percent bias.

4. Result

4.1. Changes in vegetation cover

According to the land use classification from the MODIS datasets, Fig. 2 reveals that the LP is predominated by grasslands, accounting for 67 % in 2001 and 62.3 % in 2015. Most of the forest and croplands are in the southern LP. The forest areas accounted for 7.43 % of the total area in 2001 and 9.68 % in 2015. It is considerable that 2.8 % of grasslands were removed from LP and replaced by forest lands in southeastern LP, where about 0.73 % of croplands transferred into forest lands from 2001 to 2015. In addition, 3.48 % of grasslands are replaced by croplands in the eastern LP. Contrarily, 0.34 % of croplands were converted to grasslands. The water areas are scattered, and their changes can be negligible. The barren lands are mainly distributed in the northern LP. Compared to 2001, 0.67 % of barren lands were converted into grasslands in 2015. In general, the land cover changes in LP are notable and such conversions indicate that the evolution of surface biophysical parameters will occur in the LP.

Fig. 3 presents the spatial change in the summer LAI, FVC, and albedo from 2001 to 2015. Generally, the spatial pattern of the change in FVC coincides with LAI. The FVC and LAI increase, but albedo decreases over most regions in LP in summer. The rising region of LAI and FVC accounts for 82 % of LP. On average, they increase by 0.18 m^2/m^2/decades and 5 % decades^{-1} with significant change at *F*-test ($p < 0.05$, Fig. 3d), respectively. In the central LP, a significant greening trend was observed with the magnitude of LAI 0.8–1.4 m^2/m^2/decades and FVC 25~29 % decades^{-1}. However, LAI and FVC in the Northwestern and Southeastern LP showed decreasing trends, with a value of − 1.2~− 0.4 m^2/m^2/decades and − 20 %~− 10 % decades^{-1} (Fig. 3a, b). While considering that the albedo of the forest is darker than open land (such as crops, grass, bare soil, etc.), the albedo is different between 2001 and 2015. The data showed that 95 % of albedo decreases in the LP. The summer albedo decreases by 0.016 decades^{-1} ($p < 0.05$) across the entire region. The lowest region of albedo distributes in the center and north LP, with the albedo decreasing by 0.07–0.03 decades^{-1}. However, a patchy exception to the trend can be found in the eastern LP, where the albedo increased more than 0.02 decades^{-1} (Fig. 3c). In general, the implication of the 'GTG' program in LP will modify biogeophysical parameters (including LAI, FVC, and albedo) which will provide a reference for different scenarios for the Noah modules of the WRF.

4.2. Change in temperature

The different vegetation simulations adequately captured summer climate change in the LP. Fig. 4 shows the spatial pattern of the mean near-surface air temperature variability (the difference between VGS and CTL at the pixel level) across LP caused by implementation of the 'GTG' project from 2001 to 2015. Overall, the average change in temperature response to afforestation showed a cooling effect (−0.16 °C) in summer (Fig. 4a). Moreover, the impacts of land cover change on average temperature had significant spatial features at the grids affected. A higher cooling effect occurred in the central and southern LP with a magnitude of − 0.6~− 0.8 °C. In contrast, dispersed warming signals are simulated in the Eastern LP, where deforestation was evident. It's noteworthy that a remarkable warming effect occurred in the Northern LP because the land use classification there was barren, but in 2015, some barren lands were converted to grasslands which had a lower albedo than barren lands; hence the land cover change contributed to warming through increased solar heating of land.

When focusing on afforestation effects on the average daily maximum (T_{max}) and minimum (T_{min}) surface temperature, we noticed a consistent signal decrease (Fig. 4b, c). During summer, T_{min} reduction was found with a magnitude of − 0.22 °C cooling than that of T_{max} with a magnitude of − 0.14 °C. The spatial feature of minimum temperature variations showed widespread cooling in most areas across LP. The most substantial cooling effect was observed in the LP's center, up to − 0.8 °C, while the maximum temperature decrease during summer was less noticeable compared to T_{min}, with the most cooling signal of − 0.4~− 0.6 °C in the southwestern LP. Furthermore, a slightly warming T_{max} sign was found across the Eastern LP.

A clear temporal pattern emerged from the result. The impact of land cover change on temperature was assessed in different months (Fig. 4d), and the simulations illustrated the evident summer cooling effect. It is temporally heterogeneous with an average temperature cooling up to − 0.72–0.34 °C and − 0.71–0.33 °C in June and August, and larger than in July. The average T_{max} variability response to vegetation greening in August (−0.79 to 0.50 °C) was slightly greater than in June and July. The magnitude of the cooling effect on average T_{min} in June (−0.80 to 0.24) was greater than that in July and August.

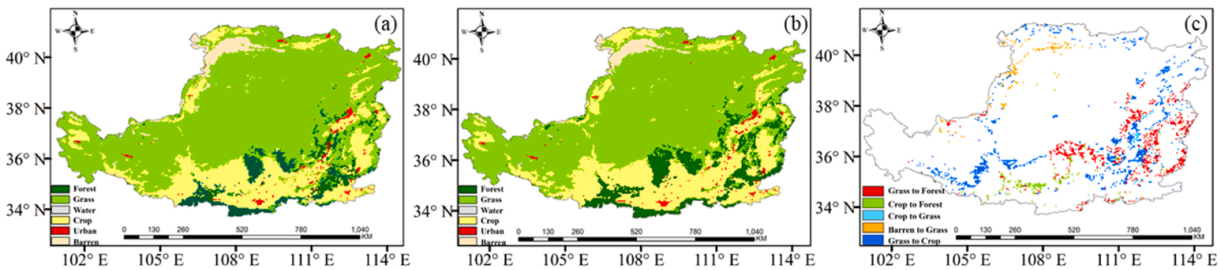

Fig. 2. Different scenarios of land cover across LP. Spatial pattern of land use in (a) 2001(CTL) (b) 2015 (SVG), and (c) land cover conversions from 2001 to 2015.

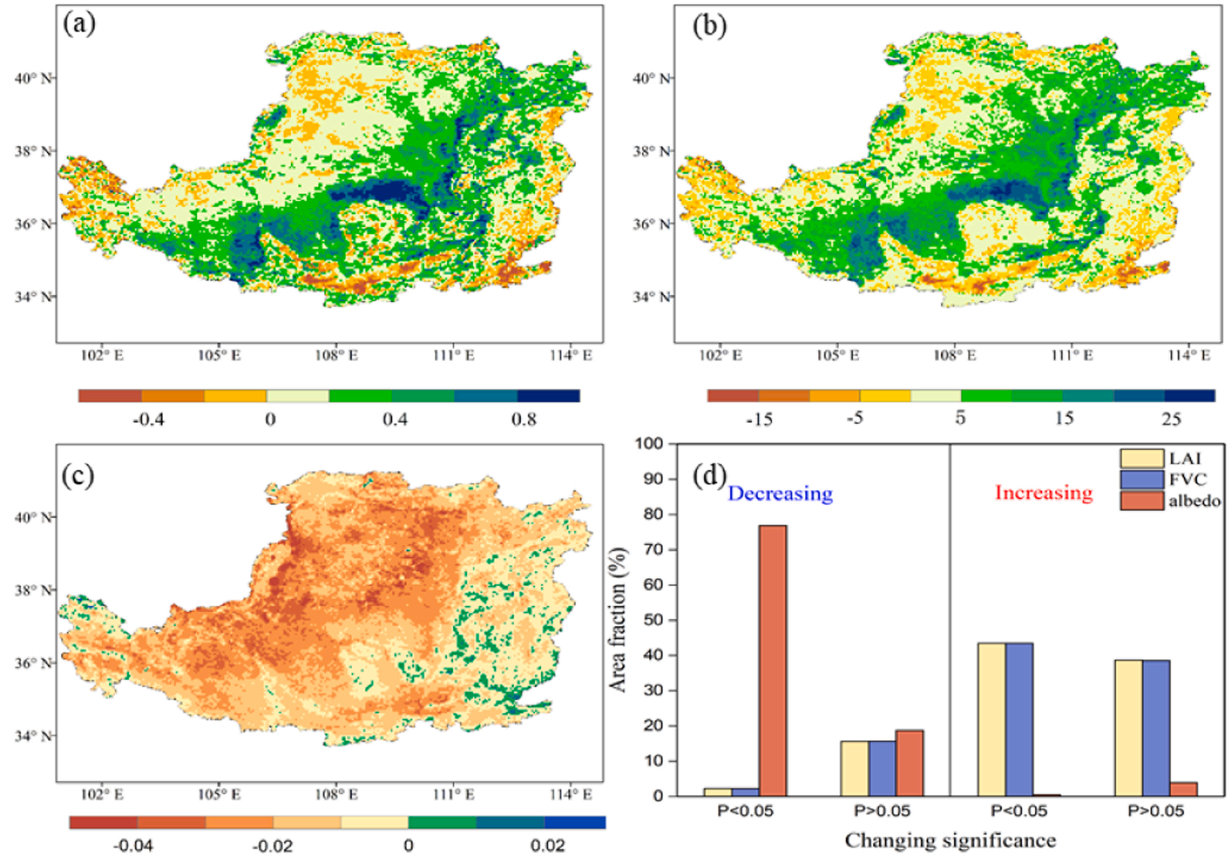

Fig. 3. Observed the decade different of (a) LAI (m^2/m^2) (b) FVC (%) and (c)albedo in LP, with the period of 2001–2015 in summer and (d) significance test (assumed for *p*-values lower than 0.5).

4.3. Change in relative humidity

Intensive and widespread afforestation in the LP has been confirmed to affect land surface heating. Meanwhile, it will modulate near-surface evaporation-ratio altering humidity. Regionally, relative humidity (*RH*) changes are uncertain (Byrne and O'Gorman, 2016). The expanded forest areas generally experience a wetting signal (increased relative humidity *RH*). Fig. 5a indicates an annual average *RH* variability of 0.67 %. Region with more than 62.6 % of the LP showed an increasing *RH* after afforestation. Results illustrated *RH* wetting effect (with the average *RH* of 3~4 %) over the dispersed central and Southern LP in response to the vegetation greening. What's more, a moderate wetting in summer daily average *RH* was found within central LP with *RH* increase by 2~3 %. However, a slight drying signal was observed in the Eastern LP. Although there was a barren transfer to grasslands in the Northern LP, the roots of the grassland cannot access deeper reservoirs of soil water (Jackson et al., 1996), which will limit the evapotranspiration leading to a decrease in relative humidity (Baldocchi et al., 2004; Santanello et al., 2009).

The increase in averaged daily minimum relative humidity (RH_{min}) was higher than the average daily maximum relative humidity (RH_{max}) (Fig. 5b, c). Averaged at all LP levels, the analysis of the RH_{max} increased by 0.36 % in summer, and 57 % of the grids showed a wetting effect. The largest value of 2 % or more was observed in the central and southern LP, while a contrasting effect can be observed in northern and eastern LP, and the RH_{max} decrease was up to − 2 % in the north LP. Compared to RH_{max}, there was a clear wetting expansion in RH_{min} (with the mean magnitude of 0.94 %), especially in eastern LP. We note that the predominantly wetting effect in RH_{min} during summer reached about 3~4 % in the central LP.

The summer *RH* increased in different months, and the most apparent wetting occurred in August between − 2.19 %~3.88 % (Fig. 5d). Similarly, the RH_{max} in August was slightly greater than in other periods, with a magnitude of − 2.30 %~3.53 %. However, the most significant rise of RH_{min} was in June, with the variability between − 2.53 %~3.36 %. Simulation of the change in surface temperature and humidity further revealed that the afforestation has a cooling and wetting effect on the land surface in LP.

4.4. Change in moist heat condition

There is an uncontroversial result that afforestation can affect surface temperature and humidity. In addition, it also has an impact on the local moist heat, thereby having far-reaching consequences. As a combined indicator, the wet-bulb temperature was used to

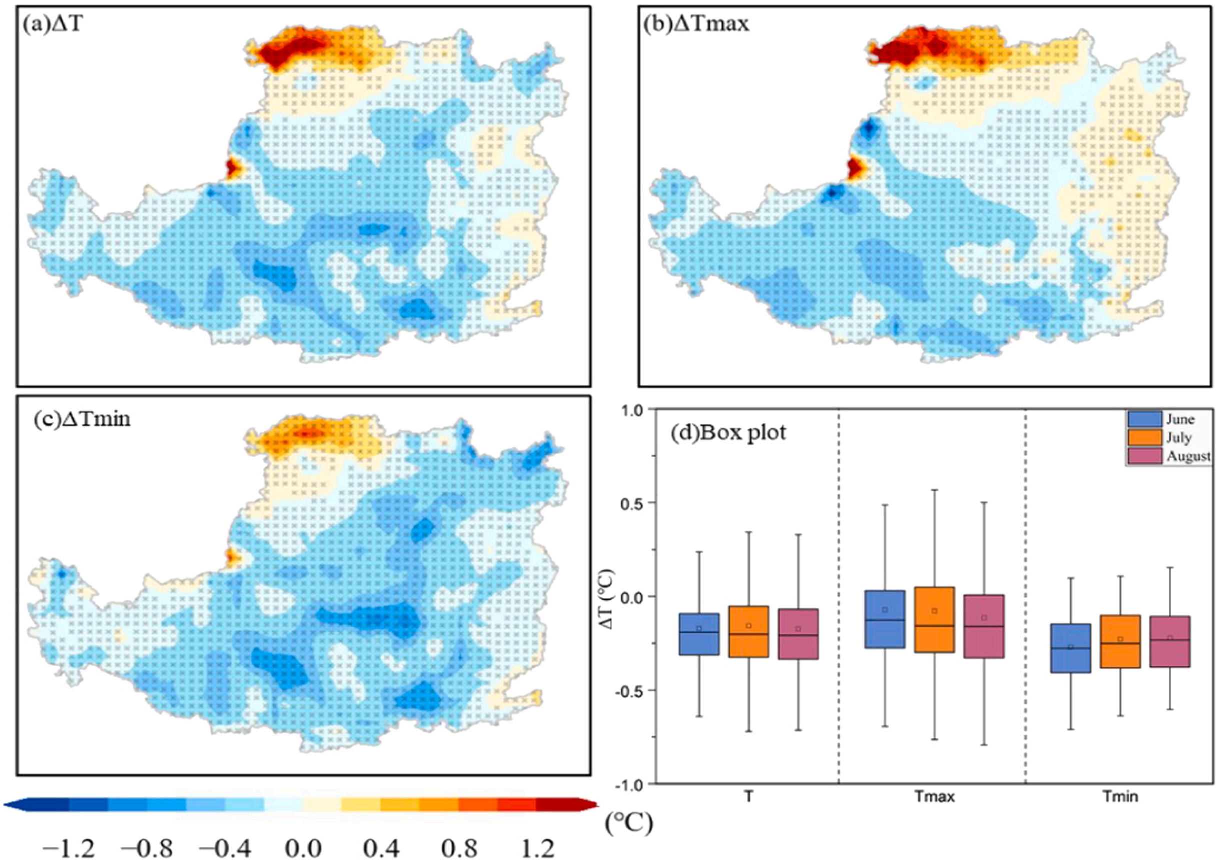

Fig. 4. The role of vegetation restoration surface temperature in summer. Spatial difference between afforestation and no-afforestation scenarios during summer for 2001–2015 for (a) average surface temperature (°C), (b) the daily maximum of surface temperature (°C), (c) the daily minimum surface temperature (°C), and (d) their Box-and-whisker plots.

describe the moist heat condition. We determined the difference in *Tw* response to VGS and CTL scenarios across LP in Fig. 6. The general pattern of annual average wet-bulb temperature (Tw_{mean}) and annual average minimum wet-bulb temperature (Tw_{min}) showed a lower moist heat after afforestation over LP. The decrease of Tw_{min} was more intense than Tw_{mean} (Fig. 6a, c). The reduction of Tw_{mean} and Tw_{min} (with the magnitude of −0.1∼−0.3 °C and −0.4∼−0.6 °C, respectively) in the central LP are slightly higher than in the remaining part. In addition, the simulation result illustrates that afforestation caused a significant change in the annual average maximum wet-bulb temperature (Tw_{max}) and influenced the moist heat environment in the LP. Decreasing Tw_{max} effects consistently spread in the western and northwestern parts of the LP. However, it was more surprising that increasing moist heat, with a magnitude restricted to 0.2 °C, was revealed in eastern and northeastern LP (Fig. 6b). Furthermore, we analyzed *Tw* variability signals through a probability function (Fig. 6d). The probability distribution of the change in Tw_{mean} and Tw_{min} peak at around − 0.2∼− 0.1 °C and − 0.05∼− 0.04 °C, respectively, while when focused on Tw_{max}, the distribution was translated into higher *Tw* with the peaks around 0.04–0.05 °C.

To investigate the wet-bulb temperature change response to relative humidity and near-surface air temperature change, we further discussed the relationship between them and disaggregated the driving factors of ΔTw (Fig. 7). The ΔTw relative to afforestation was broadly consistent with ΔT and had a significant positive correlation with ΔT, with $R^2 = 0.99$ ($P < 0.01$, *F*-test) (Fig. 7a). Fig. 7b shows that an increase in surface temperature corresponds to lower relative humidity. Since in the water-limited region, the increase rate of local vapor pressure is slower than saturated vapor pressure, leading to the shrink of relative humidity. Moreover, the change of *Tw* roughly coincides with *T*, that is to say, the cooling effect is the most predominant factor affecting the local *Tw*. The change of *Tw* roughly coincides with *T*, indicating that the cooling effect is the most predominant factor affecting the local *Tw*. In the first quadrant of Fig. 7b, although there was a significant wet-bulb temperature decrease in the region with lower surface temperature and higher relative humidity, the decreased rate in *Tw* was slower than the surface temperature because of the enhancement of relative humidity offsets the cooling effect. Moreover, the increase of *Tw* concentrates in the fourth quadrant, where the rise in surface temperature will enhance the *Tw* signal, leading to moist heat stress. Therefore, neglecting the role of relative humidity might expose humans to the risk of moist heat stress.

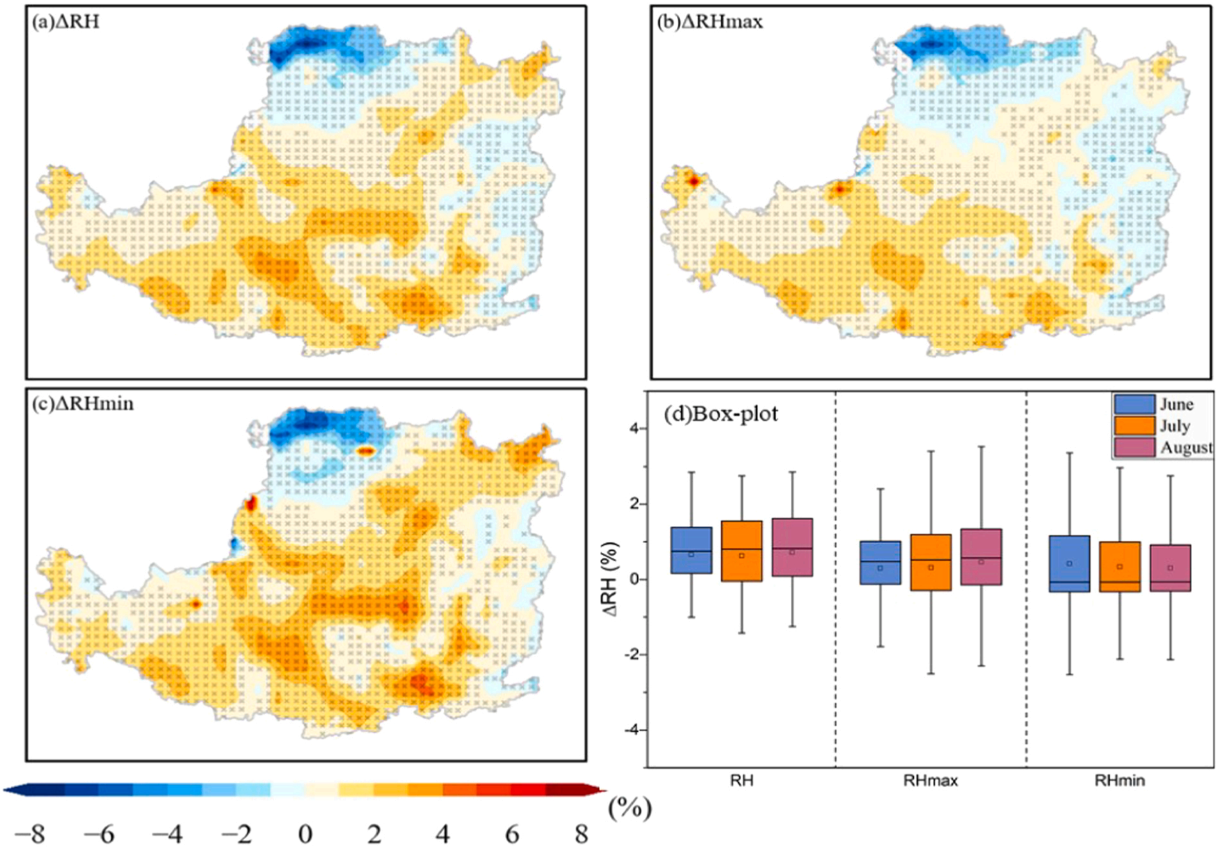

Fig. 5. Change in relative humidity in LP during summer. Spatial difference between afforestation and no-afforestation scenarios during summer for 2001–2015 for (a) average relative humidity (%), (b) the daily maximum of relative humidity (%), (c) the daily minimum relative humidity (%), and (d) their Box-and-whisker plots.

4.5. Change in the energy budget

To give insights into the dominant physical mechanisms of climate response from afforestation effects, we detected the difference in energy budget (including net radiation flux, latent heat flux, sensible heat flux, and ground heat flux) between VGS and CTL scenarios. Fig. 8a1 shows that afforestation decreased the albedo across most areas of the LP; therefore, the mean net radiation (RN_{mean}) showed an increase with the magnitude of 2.15 W.m^{-2}. The maximum of net radiation (RN_{max}) was increased by 3.57 W.m^{-2}, and the central LP of RN_{max} even increased by 10–40 W.m^{-2} (Fig. 8a2). At the same time, the minimum of net radiation (RN_{min}) changes are not remarkable (0.89 W.m^{-2}, Fig. 8a3). What's more, vegetation expansion could intensify mean latent heat flux (LH_{mean}) and maximum latent heat flux (LH_{max}), which were researched by 3.54 W.m^{-2} and 10.90 W.m^{-2}, respectively (Fig. 8b1, b3). The increase in LH_{max} (25–40 W.m^{-2}) was much more substantial than LH_{mean} (5–15 W.m^{-2}) in the region with obviously extensive vegetation (Fig. 8b2). However, a negative change in the minimum latent heat flux (LH_{min}) decreased by-1.36 W.m^{-2}. The higher LH was accompanied by a lower temperature in the atmosphere, weakening the turbulent heat exchange between land surface and atmosphere. Therefore, a negative change in sensible heat flux will appear in LP. The average sensible heat flux was weakened by − 1.10 W.m^{-2}, and the effect was evident in the central LP (−5~−10 W.m^{-2}) (Fig. 8c1). The magnitude of decrease in the maximum sensible heat flux (SH_{max}) was − 3.15 W.m^{-2} (−10~−20 W.m^{-2} in central LP, Fig. 8c2), which was larger than that of the minimum sensible heat flux (SH_{min}) (−0.62 W.m^{-2} for average SH, within 10 W.m^{-2} in most regions, Fig. 8c3). According to Fig. 9, the latent heat flux had a negative effect on wet-bulb temperature, and they don't show a strong correlation with each other due to the influence of other factors, such as albedo, wind speed, etc. On the contrary, the sensible heat flux positively affects wet-bulb temperature. Generally, the high-level change of sensible heat flux was consistent with a notable shift in wet-bulb temperature. Therefore, sensible heat flux might be the primary factor affecting the wet-bulb temperature. In addition, the ground heat flux was essential for estimating the temperature (Liang et al., 1999). Our research showed that the increase in mean ground heat flux (*GRD*) was not significant (0.15 W.m^{-2}, Fig. 8d1), and the magnitude in maximum ground heat flux (GRD_{max}) decreased by 1.28 W.m^{-2} across LP (Fig. 8d2). Minimum ground heat flux (GRD_{min}) was − 0.65 W.m^{-2} (Fig. 8d3), which means less energy was released from the soil in the nighttime, affected by vegetation greening, and it was in favor of the cooling effect (Zheng et al., 2020).

Given that the boundary-layer thickness was directly influenced by land surface and thermal change (including land cover transfer,

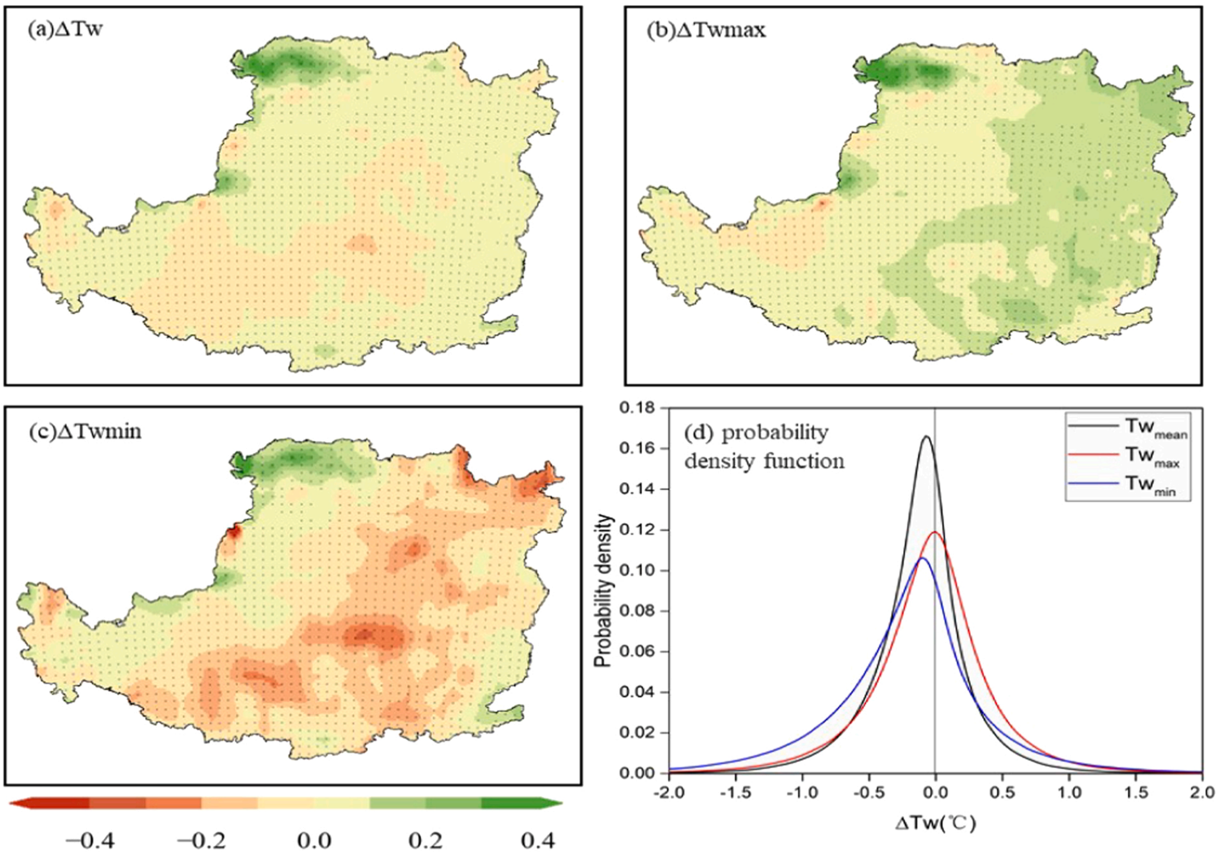

Fig. 6. Influence of afforestation on moist heat in LP during summer. Spatial differences were simulated by WRF, based on afforestation and no-afforestation scenarios for 2001–2015. (a) average wet-bulb temperature (°C), (b) the daily maximum of wet-bulb temperature (°C), (c) the daily minimum wet-bulb temperature (°C), and (d) their probability density function, show the distribution of the value.

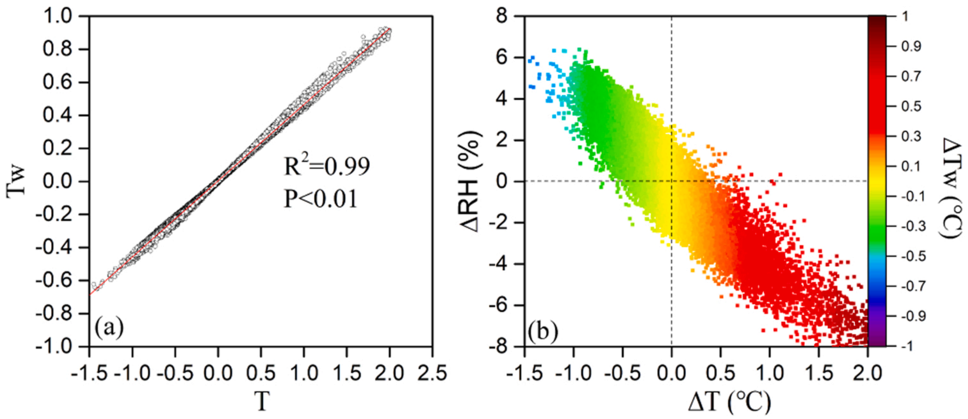

Fig. 7. Relationship between (a) the change of wet-bulb temperature and near surface air temperature and (b) the change of near surface air temperature and relative humidity, the color represents the variation of wet-bulb temperature for each pixel grids. Each point represents the year-average value on the pixel grids.

the variation of temperature and radiation, etc.), a massive reduction in the height of PBL was found during summer in the afforestation case (Fig. 10a). It was well established that the decrease of PBL (planetary boundary layer) allowed an increase of low-level moist enthalpy when no deep convection occurred (deep convection refers to the thermally driven turbulent mixing that moves air parcels from the lower to the upper atmosphere). Fig. 10b shows that afforestation developed the anticyclonic circulation in the LP, that is to say, the subsidence of PBL enhances moist enthalpy, which will increase the *Tw* in LP. In summary, afforestation alters the PBL

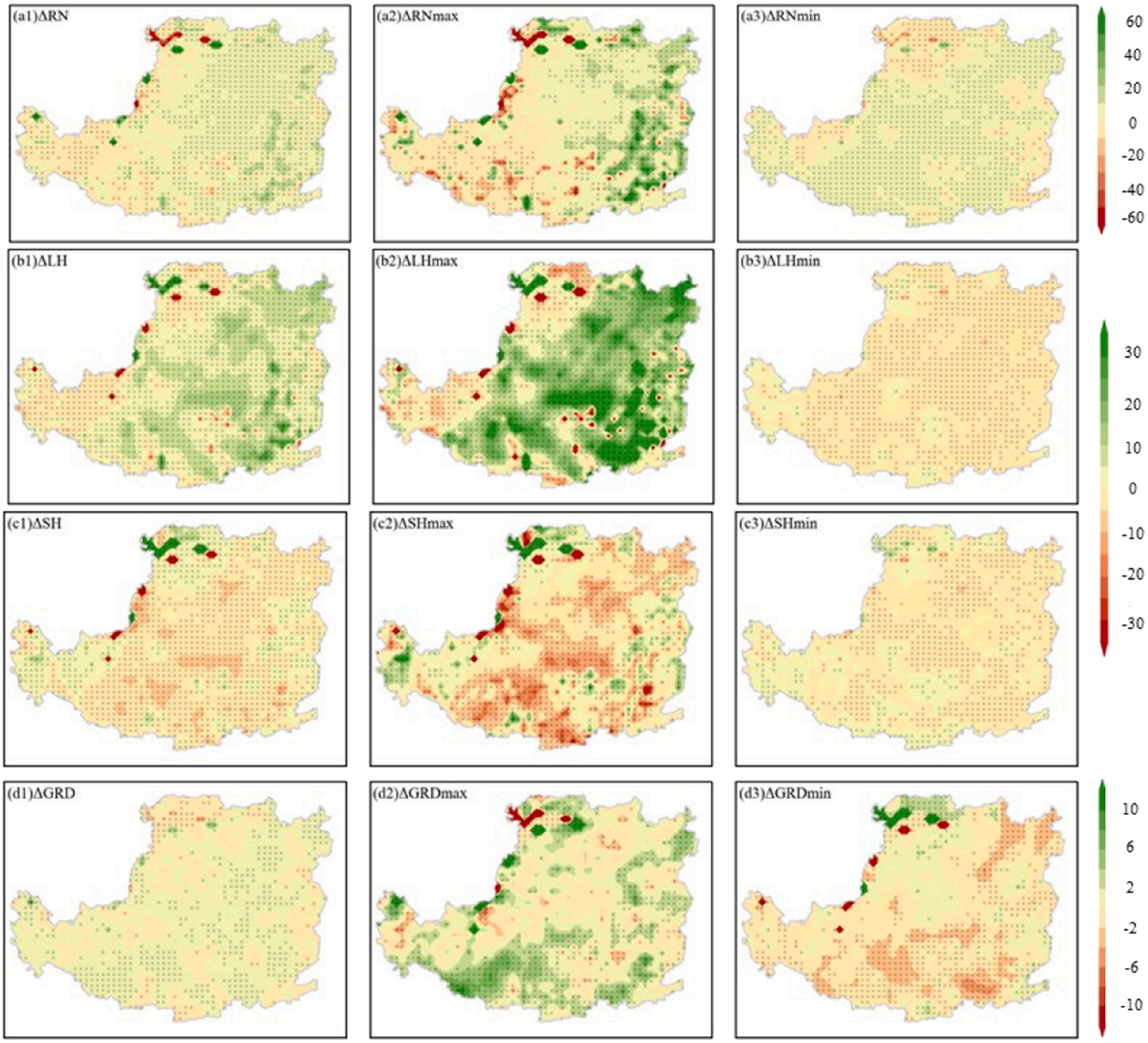

Fig. 8. Distribution of mean summer energy budget components caused by afforestation across LP. Spatial differences of average daily value, average daily maximum and average daily minimum value ($W.m^{-2}$) in (a1-a3) net radiation, (b1-b3) latent heat flux (c1-c3) sensible heat flux, and (d1-d3) ground heat flux for the period of 2001–2015.

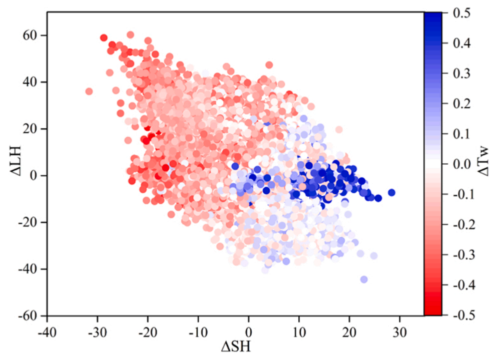

Fig. 9. Relationship of the change in latent heat flux, sensible heat flux and wet-bulb temperature.

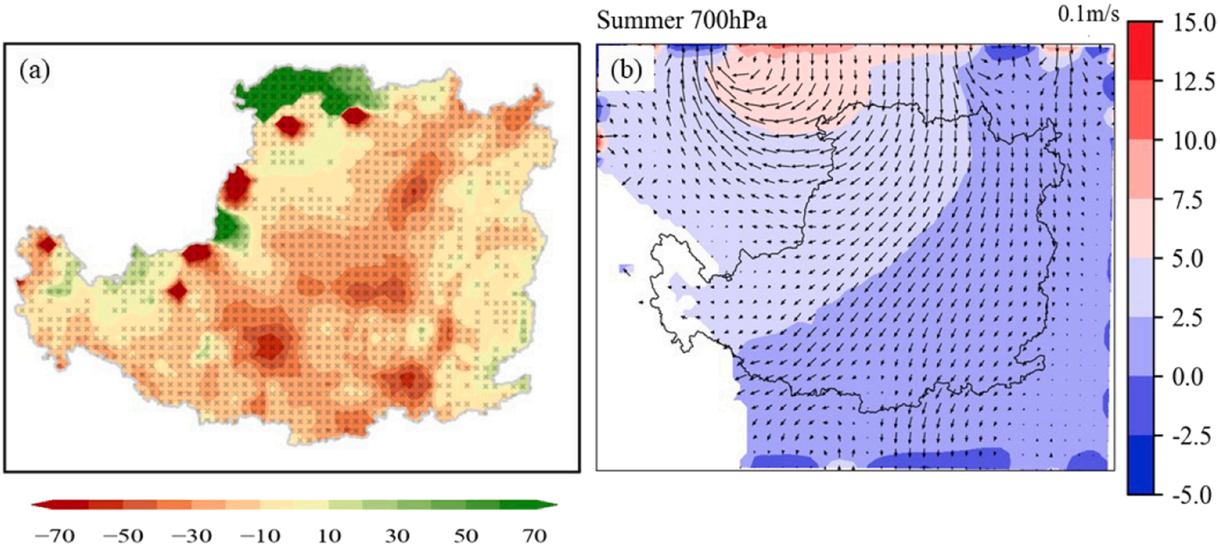

Fig. 10. (a) spatial differences (VGS minus CTL) of simulated PBL and (b) spatial differences (VGS minus CTL) of simulated geopotential height (shading, m) and wind field (vectors, m/s) at700 hPa during summer.

through the local climate factors (such as temperature and humidity) and energy budget, which will mediate the moist heat stress in LP.

5. Discussion

Vegetation has undergone conspicuous changes throughout the LP (Wang et al., 2020). This extensive vegetation greening has been instrumental in modulating surface energy partitioning, ultimately affecting the strength of land-atmosphere coupling and redistributing of heat and moisture (Cao et al., 2015). The greening dynamics and energy budget coupling in arid and semi-arid areas are stronger than in others, amplifying the relationship between climate and vegetation in arid regions rather than in other climate zones (Mallick et al., 2016*; Hoek* van Dijke et al., 2020). However, with the background of climate change, it is hard to isolate the contribution of vegetation restoration to the climate metrics variation. In this work, we quantified the response of climate change to the application of the 'GTG' program in LP and discussed their relationship with the energy budget through WRF, which helped us to understand the possible physical mechanisms for such vegetation expansions.

The surface temperature change depends on the integrated effect between net radiation and heat flux (Betts, 2011). In the LP, satellite observation showed a broad vegetation restoration. Given the lower albedo of forests (Bonan, 2008), the available energy of forests was larger than grasslands and crops, which led to a boost in RN, hence the warming effect was amplified. While the relationship between greening and surface temperature is complex, the cooling effect might suppress the warming signal in response to surface energy change between latent and sensible heat fluxes. Compared to grasslands, forests differ in the partitioning of net radiation into sensible and latent heat fluxes. In particular, in arid environments, the forests lead to a stronger plant-mediated than grasslands or croplands. Therefore, vegetation-temperature feedback in the LP is reflected by the intensified latent heat fluxes, which increase the evapotranspiration and decrease the near-surface temperature (*Baidya* et al.*, 2003*). In contrast, sensible heat flux, an alternative way to release energy, exhibited an opposite pattern with latent heat fluxes, and thus a negative sensible heat flux change appeared in the LP. Ultimately, during the transition from grasslands/croplands (CTL) to forests (VGS), Bowen ratio is used to relate the water balance to the energy balance. Specifically, the vary in evaporation will lead to obvious change in energy component (Dow and DeWalle, 2000). Bowen ratio is defined as the ration of sensible to latent heat fluxes (Comunian et al., 2018), which reflects the dry and wet condition of the ecosystem. If the Bowen ratio$>$ 1, more turbulent energy flux is released into the atmosphere as sensible heat flux, indicating a dry climate, on the contrary, if the Bowen ratio$<$ 1, indicating a humid environment (Irmak et al., 2014). In this research, the Bowen ratio decreases from 0.53 to 0.49, indicating that more latent heat flux return to the atmosphere after afforestation, which will enhance the decrease of temperature (Hu et al., 2019*,* Zhang et al., 2013). Finally, the cooling effect causes climate mitigation to counterbalance the radiation-related warming. We considered the LP's maximum and minimum energy distribution to evaluate further the role of vegetation greening in extreme conditions. Consistent with previous research, the minimum daily cooling was more widespread and pronounced than the daily maximum (Yu et al., 2020b*;* Cao et al., 2019).

The change in surface temperature and humidity influenced the region's moist heat. The increase in moist heat associated with high temperature and high humidity had a negative impact on human health (Coffel et al., 2019). The mortality and morbidity, especially for people with cardiovascular and respiratory diseases, are significantly associated with a high moist heat environment (*Pal* et al.*, 2016;* Mishra et al., 2020). Emerging studies have raised attention to the change in moist heat stress (Chen et al., 2020). Long-lasting, more intense, and frequent moist heat conditions occurred on the 21st, and the most significant increase in moist heat stress was witnessed in the tropical region (Coffel et al., 2018). Furthermore, the anthropogenic influence substantially enhances a hotter and wetter environment, such as irrigation (Cook et al., 2015) and urbanization (Luo and Lau, 2021). With the expansion of the LP forest, the near-surface air temperature, relative humidity, and moist heat stress have changed. Based on wet bulb temperature, we demonstrate the response of moist heat conditions to afforestation and reveal the spatiotemporal characteristic and physical mechanisms of moist heat. The results illustrated that the surface temperature and relative humidity showed an opposing interaction with wet bulb temperature. Compared to the dry bulb temperature, the variability of relative humidity dampens *Tw*, and the wetting effect may partly offset the impact of amplified cooling on *Tw*. Consequently, the increases in wet bulb temperature and dry bulb temperature do not occur simultaneously. Although vegetation expansion dampens the rise in surface temperature in most areas of LP, the wet bulb temperature on daily maximum did not decrease in part of LP, reflecting the combined effect of increasing humidity and decreasing temperature. Here, some researchers showed that the increasing wet-bulb temperature would exceed the threshold value and human tolerance over the specific region in the future (Coffel et al., 2018; Pal and Eltahir, 2016), which will make widespread exposure to humans to moist heat stress condition. Thus, prevention and management of the humid-heat risks are essential for human health.

Our study has detected how afforestation influences climate and to what degree they affect climatic elements through the modification of biophysical processes. While the biogeochemical process has been ignored. The vegetation absorbs carbon dioxide, influencing the terrestrial climate through climate-radiative and vegetation-physiological forcing. Therefore, the climate response to vegetation greening should link the potential carbon sequestration to the terrestrial energy balance (Huang et al., 2018). Afforestation is presented as an effective solution to mitigate climate change. However, with the expansion of vegetation, there might be a complex change in the regional climate factors (Feng et al., 2016; Ge et al., 2020; Cao et al., 2019). In the water-limited region, widespread overplanting proved more evaporation, leading to soil drying (Zhang and Liang, 2018) and decreasing regional water availability (Sterling, et al., 2013), which exacerbates the water shortage (Lv et al., 2019). While, in the water-rich region, the large scale of revegetation may increase moist heat stress. Therefore, it is worth further exploring what the reasonable vegetation scope is.

6. Conclusion

Applying the ’GTG’ program enables the greening condition of the LP. Changes in land cover alter local land surface biophysical processes and disturb energy fluxes, thereby affecting regional climate conditions. To identify the different land cover, we performed two sets of simulations. One considered vegetation greening scenario (VGS); one was a control scenario (CTL). And then simulated the regional climate responses to afforestation using the regional land-atmosphere interaction model-WRF. Moreover, the wet bulb temperature (*Tw*) was discussed to underscore the moist heat, and we assessed the moist heat effect from the perspective of water and energy balance.

The result reveals that after the afforestation, the temperature decreased in most areas across LP. A higher cooling effect could be observed in the central and southern LP with a magnitude of $-0.6\sim-0.8$ °C. The region with more than 62.6 % of the LP showed an increasing *RH*, with the average *RH* variability of 0.67 %. Furthermore, after the calculation of *Tw*, this research illustrates that the *Tw* and Tw_{min} showed a lower moist heat stress after afforestation with the magnitude of $-0.1\sim-0.3$ °C and $-0.4\sim-0.6$ °C, respectively. However, its ratio was slower than surface temperature caused by relative humidity. An increasing signal occurred in Tw_{max}, especially in the Eastern LP (restricted to 0.2 °C), which might expose human health to an awful environment. Moreover, to investigate the dominant physical mechanisms of the climate response from afforestation, we detect the difference in energy budget. The result shows that the afforestation decreased the albedo, therefore the mean net radiation increased after afforestation. As a significant part of energy balance, the sensible heat flux was weekend by -1.10 W.m^{-2}, and its change was highly consistent with *Tw,* which might be the primary factor affecting the moist heat stress.

In general, afforestation might have a negative impact on moist heat stress. However, current climate policy deploying frameworks ignore the surface biophysical effect on climate leading to high risk for agriculture and society. This research identified the lower atmosphere consequences of afforestation, which will supply scientific evidence for policy-making processes and refine climate adaptation strategies.

CRediT authorship contribution statement

Zhang Shulin: Conceptualization, Methodology, Formal analysis, Writing – original draft, Writing – review & editing. **Wang Weiguang:** Validation, Supervision, Funding acquisition. **Adriaan J. Teuling:** Writing – review & editing, Supervision, Validation. **Liu Guoshuai:** Software, Data curation. **Olusola O. Ayantobo:** Writing – review & editing. **Fu Jianyu:** Writing – review & editing. **Dong Qing:** Writing – review & editing.

Declaration of Competing Interest

The authors declare that they have no known competing financial interests or personal relationships that could have appeared to influence the work reported in this paper.

Data Availability

The authors are unable or have chosen not to specify which data has been used.

Acknowledgments

This work was jointly supported by the National Natural Science Foundation of China (No. 51979071, 51779073), the Distinguished Young Fund Project of Jiangsu Natural Science Foundation (No. BK20180021), the National Key Research and Development Program of China (No. 2018YFA0605402), the National "Ten Thousand Program" Youth Talent and the Six Talent Peaks Project in Jiangsu Province, the Priority Academic Program Development of Jiangsu Higher Education Institutions (PAPD), the Fundamental Research Funds for the Central Universities (No. B200204016), and China Scholar Council (No. 202106710118).

Meanwhile, thanks to several institutions for making their data freely available. The authors thank the anonymous reviewers and the journal's Editorial board.

Appendix A. Supporting information

Supplementary data associated with this article can be found in the online version at doi:10.1016/j.ejrh.2022.101209.

References

Abiodun, B.J., Salami, A.T., Matthew, O.J., Odedokun, S., 2013. Potential impacts of afforestation on climate change and extreme events in Nigeria. Clim. Dyn. 41 (2), 277–293. https://doi.org/10.1007/s00382-012-1523-9.

Alkama, R., Cescatti, A., 2016. Biophysical climate impacts of recent changes in global forest cover. Science 351 (6273), 600–604. https://doi.org/10.1126/science.aac8083.

Baldocchi, D.D., Xu, L.K., Kiang, N., 2004. How plant functional-type, weather, seasonal drought, and soil physical properties alter water and energy fluxes of an oak-grass savanna and an annual grassland. Agric. . Meteorol. 123 (1–2), 13–39. https://doi.org/10.1016/j.agrformet.2003.11.006.

Balsamo, G., et al., 2015. ERA-Interim/Land: a global land surface reanalysis data set. Hydrol. Earth Syst. Sci. 19 (1), 389–407. https://doi.org/10.5194/hess-19-389-2015.

Betts, R.A., 2000. Offset of the potential carbon sink from boreal forestation by decreases in surface albedo. Nature 408 (6809), 187–190. https://doi.org/10.1038/35041545.

Betts, R.A., 2011. Climate science Afforestation cools more or less. Nat. Geosci. 4 (8), 504–505. https://doi.org/10.1038/ngeo1223.

Bonan, G.B., 2008. Forests and climate change: forcings, feedbacks, and the climate benefits of forests. Science 320 (5882), 1444–1449. https://doi.org/10.1126/science.1155121.

Bright, R.M., Zhao, K.G., Jackson, R.B., Cherubini, F., 2015. Quantifying surface albedo and other direct biogeophysical climate forcings of forestry activities. Glob. Change Biol. 21 (9), 3246–3266. https://doi.org/10.1111/gcb.12951.

Byrne, M.P., O'Gorman, P.A., 2016. Understanding decreases in land relative humidity with global warming: conceptual model and GCM simulations. J. Clim. 29 (24), 9045–9061. https://doi.org/10.1175/jcli-d-16-0351.1.

Cao, Q., Yu, D.Y., Georgescu, M., Han, Z., Wu, J.G., 2015. Impacts of land use and land cover change on regional climate: a case study in the agro-pastoral transitional zone of China. Environ. Res. Lett. 10 (12), 12. https://doi.org/10.1088/1748-9326/10/12/124025.

Cao, Q., Wu, J.G., Yu, D.Y., Wang, W., 2019. The biophysical effects of the vegetation restoration program on regional climate metrics in the Loess Plateau, China. Agric. . Meteorol. 268, 169–180. https://doi.org/10.1016/j.agrformet.2019.01.022.

Cao, Z., Li, Y.R., Liu, Y.S., Chen, Y.F., Wang, Y.S., 2018. When and where did the Loess Plateau turn "green"? analysis of the tendency and breakpoints of the normalized difference vegetation index. Land Degrad. Dev. 29 (1), 162–175. https://doi.org/10.1002/ldr.2852.

Cardoso, R.M., Soares, P.M.M., Miranda, P.M.A., Belo-Pereira, M., 2013. WRF high resolution simulation of Iberian mean and extreme precipitation climate. Int. J. Climatol. 33 (11), 2591–2608. https://doi.org/10.1002/joc.3616.

Chen, L., Ma, Z.G., Zhao, T.B., 2017. Modeling and analysis of the potential impacts on regional climate due to vegetation degradation over arid and semi-arid regions of China. Clim. Change 144 (3), 461–473. https://doi.org/10.1007/s10584-016-1847-2.

Chen, L.D., Wei, W., Fu, B.J., Lu, Y.H., 2007. Soil and water conservation on the Loess Plateau in China: review and perspective. Prog. Phys. Geogr. 31 (4), 389–403. https://doi.org/10.1177/0309133307081290.

Chen, X., et al., 2020. Changes in global and regional characteristics of heat stress waves in the 21st Century. Earth Future 8 (11), 17. https://doi.org/10.1029/2020ef001636.

Cherubini, F., Huang, B., Hu, X.P., Tolle, M.H., Stromman, A.H., 2018. Quantifying the climate response to extreme land cover changes in Europe with a regional model. Environ. Res. Lett. 13 (7), 12. https://doi.org/10.1088/1748-9326/aac794.

Chotamonsak, C., Salathe, E.P., Kreasuwan, J., Chantara, S., Siriwitayakorn, K., 2011. Projected climate change over Southeast Asia simulated using a WRF regional climate model. Atmos. Sci. Lett. 12 (2), 213–219. https://doi.org/10.1002/asl.313.

Coffel, E.D., Horton, R.M., de Sherbinin, A., 2018. Temperature and humidity based projections of a rapid rise in global heat stress exposure during the 21st century. Environ. Res. Lett. 13 (1), 9. https://doi.org/10.1088/1748-9326/aaa00e.

Coffel, E.D., Horton, R.M., Winter, J.M., Mankin, J.S., 2019. Nonlinear increases in extreme temperatures paradoxically dampen increases in extreme humid-heat. Environ. Res. Lett. 14 (8), 10. https://doi.org/10.1088/1748-9326/ab28b7.

Comunian, A., Giudici, M., Landoni, L., Pugnaghi, S., 2018. Improving Bowen-ratio estimates of evaporation using a rejection criterion and multiple-point statistics. J. Hydrol. 563, 43–50. https://doi.org/10.1016/j.jhydrol.2018.05.050.

Cook, B.I., Shukla, S.P., Puma, M.J., Nazarenko, L.S., 2015. Irrigation as an historical climate forcing. Clim. Dyn. 44 (5–6), 1715–1730. https://doi.org/10.1007/s00382-014-2204-7.

Davies-Jones, R., 2008. An efficient and accurate method for computing the wet-bulb temperature along pseudoadiabats. Mon. Weather Rev. 136 (7), 2764–2785. https://doi.org/10.1175/2007mwr2224.1.

Davin, E.L., de Noblet-Ducoudre, N., 2010. Climatic Impact of Global-Scale Deforestation: Radiative versus Nonradiative Processes. J. Clim. 23 (1), 97–112. https://doi.org/10.1175/2009jcli3102.1.

Davis, R.E., McGregor, G.R., Enfield, K.B., 2016. Humidity: a review and primer on atmospheric moisture and human health. Environ. Res. 144, 106–116. https://doi.org/10.1016/j.envres.2015.10.014.

Decker, M., et al., 2012. Evaluation of the reanalysis products from GSFC, NCEP, and ECMWF using flux tower observations. J. Clim. 25 (6), 1916–1944. https://doi.org/10.1175/jcli-d-11-00004.1.

Dee, D.P., et al., 2011. The ERA-Interim reanalysis: configuration and performance of the data assimilation system. Q. J. R. Meteorol. Soc. 137 (656), 553–597. https://doi.org/10.1002/qj.828.

Deng, Y.H., et al., 2020. Comparison of soil moisture products from microwave remote sensing, land model, and reanalysis using global ground observations. Hydrol. Process. 34 (3), 836–851. https://doi.org/10.1002/hyp.13636.

Dow, C.L., DeWalle, D.R., 2000. Trends in evaporation and Bowen ratio on urbanizing watersheds in eastern United States. Water Resour. Res. 36 (7), 1835–1843. https://doi.org/10.1029/2000wr900062.

Dunne, J.P., Stouffer, R.J., John, J.G., 2013. Reductions in labour capacity from heat stress under climate warming. Nat. Clim. Chang. 3 (6), 563–566. https://doi.org/10.1038/nclimate1827.

Feng, X.M., et al., 2016. Revegetation in China's Loess Plateau is approaching sustainable water resource limits (-+). Nat. Clim. Chang. 6 (11), 1019. https://doi.org/10.1038/nclimate3092.

Feng, X.M., Fu, B.J., Lu, N., Zeng, Y., Wu, B.F., 2013. How ecological restoration alters ecosystem services: an analysis of carbon sequestration in China's Loess Plateau. Sci. Rep. 3, 5. https://doi.org/10.1038/srep02846.

Forzieri, G., Alkama, R., Miralles, D.G., Cescatti, A., 2017. Satellites reveal contrasting responses of regional climate to the widespread greening of Earth. Science 356 (6343), 1140–1144. https://doi.org/10.1126/science.aal1727.

Freychet, N., Tett, S.F.B., Yan, Z.W., Li, Z., 2020. Underestimated change of wet-bulb temperatures over east and South China. Geophys. Res. Lett. 47 (3), 7. https://doi.org/10.1029/2019gl086140.

Friedl, M.A., et al., 2002. Global land cover mapping from MODIS: algorithms and early results. Remote Sens. Environ. 83 (1–2), 287–302. https://doi.org/10.1016/s0034-4257(02)00078-0.

Ge, J., et al., 2019. The nonradiative effect dominates local surface temperature change caused by afforestation in China. J. Clim. 32 (14), 4445–4471. https://doi.org/10.1175/jcli-d-18-0772.1.

Ge, J., Pitman, A.J., Guo, W.D., Zan, B.L., Fu, C.B., 2020. Impact of revegetation of the Loess Plateau of China on the regional growing season water balance. Hydrol. Earth Syst. Sci. 24 (2), 515–533. https://doi.org/10.5194/hess-24-515-2020.

Gibbard, S., Caldeira, K., Bala, G., Phillips, T.J., Wickett, M., 2005. Climate effects of global land cover change. Geophys. Res. Lett. 32 (23), 4. https://doi.org/10.1029/2005gl024550.

Han, Z.M., et al., 2021. Spatial-temporal dynamics of agricultural drought in the Loess Plateau under a changing environment: Characteristics and potential influencing factors. Agric. Water Manag. 244, 12. https://doi.org/10.1016/j.agwat.2020.106540.

Hoek Dijke, van, et al., 2022. Shifts in regional water availability due to global tree restoration. Nature Geoscience 15 (5), 363–368. https://doi.org/10.1038/s41561-022-00935-0.

Hu, J.Y., et al., 2021. Impacts of land-use conversions on the water cycle in a typical watershed in the southern Chinese Loess Plateau. J. Hydrol. 593, 16. https://doi.org/10.1016/j.jhydrol.2020.125741.

Hu, X.P., Huang, B., Cherubini, F., 2019. Impacts of idealized land cover changes on climate extremes in Europe. Ecol. Indic. 104, 626–635. https://doi.org/10.1016/j.ecolind.2019.05.037.

Huang, B., et al., 2020. Predominant regional biophysical cooling from recent land cover changes in Europe. Nat. Commun. 11 (1), 13. https://doi.org/10.1038/s41467-020-14890-0.

Huang, L., Zhai, J., Liu, J.Y., Sun, C.Y., 2018. The moderating or amplifying biophysical effects of afforestation on CO_2-induced cooling depend on the local background climate regimes in China. Agric. 260, 193–203. https://doi.org/10.1016/j.agrformet.2018.05.020.

Irmak, S., Skaggs, K.E., Chatterjee, S., 2014. A review of the Bowen ratio surface energy balance method for quantifying evapotranspiration and other energy fluxes. Trans. ASABE 57 (6), 1657–1674. https://doi.org/10.13031/trans.57.10686.

Jach, L., Warrach-Sagi, K., Ingwersen, J., Kaas, E., Wulfmeyer, V., 2020. Land cover impacts on land-atmosphere coupling strength in climate simulations With WRF Over Europe. J. Geophys. Res. -Atmos. 125 (18), 21. https://doi.org/10.1029/2019jd031989.

Jackson, R.B., et al., 1996. A global analysis of root distributions for terrestrial biomes. Oecologia 108 (3), 389–411. https://doi.org/10.1007/bf00333714.

Jiang, X.N., Waliser, D.E., Li, J.L., Woods, C., 2011. Vertical cloud structures of the boreal summer intraseasonal variability based on CloudSat observations and ERA-interim reanalysis. Clim. Dyn. 36 (11–12), 2219–2232. https://doi.org/10.1007/s00382-010-0853-8.

Kang, S., Eltahir, E.A.B., 2018. North China Plain threatened by deadly heatwaves due to climate change and irrigation. Nat. Commun. 9, 9. https://doi.org/10.1038/s41467-018-05252-y.

Keenan, T.F., et al., 2016. Recent pause in the growth rate of atmospheric CO_2 due to enhanced terrestrial carbon uptake. Nat. Commun. 7, 9. https://doi.org/10.1038/ncomms13428.

Kerr, R.A., 2007. Global warming is changing the world. Science 316 (5822), 188–190. https://doi.org/10.1126/science.316.5822.188.

Kjellstrom, T. et al., 2016. Heat, Human Performance, and Occupational Health: A Key Issue for the Assessment of Global Climate Change Impacts. In: Fielding, J.E. (Ed.), Annual Review of Public Health, Vol 37. Annual Review of Public Health. Annual Reviews, Palo Alto, pp. 97–112. DOI:⟨10.1146/annurev-publhealth-032315–021740⟩.

Knist, S., Goergen, K., Simmer, C., 2020. Evaluation and projected changes of precipitation statistics in convection-permitting WRF climate simulations over Central Europe. Clim. Dyn. 55 (1–2), 325–341. https://doi.org/10.1007/s00382-018-4147-x.

Kong, D.X., Miao, C.Y., Wu, J.W., Zheng, H.Y., Wu, S.H., 2020. Time lag of vegetation growth on the Loess Plateau in response to climate factors: Estimation, distribution, and influence. Sci. Total Environ. 744, 11. https://doi.org/10.1016/j.scitotenv.2020.140726.

Koteswara K, R., et al., 2020. *Projections of heat stress and associated work performance over India in response to global warming.* Sci Rep 10 (16675). https://doi.org/10.1038/s41598-020-73245-3.

Lansu, E.M., van Heerwaarden, C.C., Stegehuis, A.I., Teuling, A.J., 2020. Atmospheric aridity and apparent soil moisture drought in european forest during heat waves. Geophys. Res. Lett. 47 (6), 8. https://doi.org/10.1029/2020gl087091.

Li, Y., et al., 2015. Local cooling and warming effects of forests based on satellite observations. Nat. Commun. 6, 6603. https://doi.org/10.1038/ncomms7603.

Li, Y., et al., 2016. The role of spatial scale and background climate in the latitudinal temperature response to deforestation. Earth Syst. Dynam. 7 (1), 167–181. https://doi.org/10.5194/esd-7-167-2016.

Liang, S.L., et al., 2013. A long-term Global LAnd Surface Satellite (GLASS) data-set for environmental studies. Int. J. Digit. Earth 6, 5–33. https://doi.org/10.1080/17538947.2013.805262.

Liang, X., Wood, E.F., Lettenmaier, D.P., 1999. Modeling ground heat flux in land surface parameterization schemes. J. Geophys. Res. -Atmos. 104 (D8), 9581–9600. https://doi.org/10.1029/98jd02307.

Liu, Z.J., et al., 2018. Evaluation of spatial and temporal performances of ERA-interim precipitation and temperature in mainland China. J. Clim. 31 (11), 4347–4365. https://doi.org/10.1175/jcli-d-17-0212.1.

Liu, Z.P., Wang, Y.Q., Shao, M.G., Jia, X.X., Li, X.L., 2016. Spatiotemporal analysis of multiscalar drought characteristics across the Loess Plateau of China. J. Hydrol. 534, 281–299. https://doi.org/10.1016/j.jhydrol.2016.01.003.

Luo, M., Lau, N.C., 2021. Increasing human-perceived heat stress risks exacerbated by urbanization in China: a comparative study based on multiple metrics. Earth Future 9 (7), 13. https://doi.org/10.1029/2020ef001848.

Lv, M.X., Ma, Z.G., Li, M.X., Zheng, Z.Y., 2019. Quantitative analysis of terrestrial water storage changes under the grain for green program in the Yellow River Basin. J. Geophys. Res. -Atmos. 124 (3), 1336–1351. https://doi.org/10.1029/2018jd029113.

Mallick, K., et al., 2016. Canopy-scale biophysical controls of transpiration and evaporation in the Amazon basin. Hydrol. Earth Syst. Sci. 20 (10), 4237–4264. https://doi.org/10.5194/hess-20-4237-2016.

Mishra, V., et al., 2020. Moist heat stress extremes in India enhanced by irrigation. Nat. Geosci. 13 (11), 722. https://doi.org/10.1038/s41561-020-00650-8.

Ning, G.C. et al., Dominant modes of summer wet bulb temperature in China. Clim. Dyn.: 16. DOI:⟨10.1007/s00382–021-06051-w⟩.

Norman, J.M., Kustas, W.P., Humes, K.S., 1995. Source approach for estimating soil and vegetation energy fluxes in observations of directional radiometric surface temperature. Agric. . Meteorol. 77 (3–4), 263–293. https://doi.org/10.1016/0168-1923(95)02265-y.

Odoulami, R.C., Abiodun, B.J., Ajayi, A.E., 2019. Modelling the potential impacts of afforestation on extreme precipitation over West Africa. Clim. Dyn. 52 (3–4), 2185–2198. https://doi.org/10.1007/s00382-018-4248-6.

Office of the National Greening Committee, 2019. Bulletin on the state of land greening in China in 2018. Land Green. 20 (3), 10–13.

Pal, J.S., Eltahir, E.A.B., 2016. Future temperature in southwest Asia projected to exceed a threshold for human adaptability. Nat. Clim. Chang. 6 (2), 197–200. https://doi.org/10.1038/nclimate2833.

Peng, S.S. et al., 2014. Afforestation in China cools local land surface temperature. Proc. Natl. Acad. Sci. U. S. A., 111(8): 2915–2919. DOI:⟨10.1073/pnas.1315126111⟩.

Qu, L.L., Huang, Y.X., Yang, L.F., Li, Y.R., 2020. Vegetation restoration in response to climatic and anthropogenic changes in the Loess Plateau, China. Chin. Geogr. Sci. 30 (1), 89–100. https://doi.org/10.1007/s11769-020-1093-4.

Rao, K.K., et al., 2020. Projections of heat stress and associated work performance over India in response to global warming. Sci. Rep. 10 (1), 14. https://doi.org/10.1038/s41598-020-73245-3.

Raymond, C., Singh, D., Horton, R.M., 2017. Spatiotemporal patterns and synoptics of extreme wet-bulb temperature in the contiguous United States. J. Geophys. Res. -Atmos. 122 (24), 13108–13124. https://doi.org/10.1002/2017jd027140.

Safieddine, S., Clerbaux, C., Clarisse, L., Whitburn, S., Eltahir, E.A.B., 2022. Present and future land surface and wet bulb temperatures in the Arabian Peninsula. Environ. Res. Lett. 17 (4), 9. https://doi.org/10.1088/1748-9326/ac507c.

Santanello, J.A., Peters-Lidard, C.D., Kumar, S.V., Alonge, C., Tao, W.K., 2009. A modeling and observational framework for diagnosing local land-atmosphere coupling on diurnal time scales. J. Hydrometeorol. 10 (3), 577–599. https://doi.org/10.1175/2009jhm1066.1.

Sherwood, S.C., 2018. How important is humidity in heat stress? J. Geophys. Res. -Atmos. 123 (21), 11808–11810. https://doi.org/10.1029/2018jd028969.

Shi, W.Z., et al., 2020. Dry and wet combination dynamics and their possible driving forces in a changing environment. J. Hydrol. 589, 10. https://doi.org/10.1016/j.jhydrol.2020.125211.

Srinivas, C.V., et al., 2013. Simulation of the Indian summer monsoon regional climate using advanced research WRF model. Int. J. Climatol. 33 (5), 1195–1210. https://doi.org/10.1002/joc.3505.

Stegehuis, A.I., et al., 2015. An observation-constrained multi-physics WRF ensemble for simulating European mega heat waves. Geosci. Model Dev. 8 (7), 2285–2298. https://doi.org/10.5194/gmd-8-2285-2015.

Sterling, S.M., Ducharne, A., Polcher, J., 2013. The impact of global land-cover change on the terrestrial water cycle. Nat. Clim. Chang. 3 (4), 385–390. https://doi.org/10.1038/nclimate1690.

Su, H., Wood, E.F., McCabe, M.F., Su, Z., 2007. Evaluation of remotely sensed evapotranspiration over the CEOP EOP-1 reference sites. J. Meteorol. Soc. Jpn. 85A, 439–459. https://doi.org/10.2151/jmsj.85A.439.

Sylla, M.B., Pal, J.S., Wang, G.L.L., Lawrence, P.J., 2016. Impact of land cover characterization on regional climate modeling over West Africa. Clim. Dyn. 46 (1–2), 637–650. https://doi.org/10.1007/s00382-015-2603-4.

Teuling, A.J., et al., 2010. Contrasting response of European forest and grassland energy exchange to heatwaves. Nat. Geosci. 3 (10), 722–727. https://doi.org/10.1038/ngeo950.

Teuling, A.J., et al., 2019. Climate change, reforestation/afforestation, and urbanization impacts on evapotranspiration and streamflow in Europe. Hydrol. Earth Syst. Sci. 23 (9), 3631–3652. https://doi.org/10.5194/hess-23-3631-2019.

van Dijke, A.J.H., et al., 2020. Examining the link between vegetation leaf area and land-atmosphere exchange of water, energy, and carbon fluxes using FLUXNET data. Biogeosciences 17 (17), 4443–4457. https://doi.org/10.5194/bg-17-4443-2020.

van Heerwaarden, C.C., Teuling, A.J., 2014. Disentangling the response of forest and grassland energy exchange to heatwaves under idealized land-atmosphere coupling. Biogeosciences 11 (21), 6159–6171. https://doi.org/10.5194/bg-11-6159-2014.

Wang, Y.H., et al., 2018. Major forest increase on the Loess Plateau, China (2001-2016. Land Degrad. Dev. 29 (11), 4080–4091. https://doi.org/10.1002/ldr.3174.

Wang, Y.H., et al., 2020. Do afforestation projects increase core forests? evidence from the Chinese Loess Plateau. Ecol. Indic. 117, 11. https://doi.org/10.1016/j.ecolind.2020.106558.

Wu, D., et al., 2019. Ecosystem services changes between 2000 and 2015 in the Loess Plateau, China: a response to ecological restoration. PLoS One 14 (1), 16. https://doi.org/10.1371/journal.pone.0209483.

Wu, H.C., Yang, Q.L., Liu, J.M., Wang, G.Q., 2020. A spatiotemporal deep fusion model for merging satellite and gauge precipitation in China. J. Hydrol. 584, 10. https://doi.org/10.1016/j.jhydrol.2020.124664.

Xiao, J.F., 2014. Satellite evidence for significant biophysical consequences of the "Grain for Green" Program on the Loess Plateau in China. J. Geophys. Res. -Biogeosci 119 (12), 2261–2275. https://doi.org/10.1002/2014jg002820.

Xiao, X.X., Zhang, T.J., Zhong, X.Y., Shao, W.W., Li, X.D., 2018. Support vector regression snow-depth retrieval algorithm using passive microwave remote sensing data. Remote Sens. Environ. 210, 48–64. https://doi.org/10.1016/j.rse.2018.03.008.

Xu, Y.Y., Ramanathan, V., Victor, D.G., 2018. Global warming will happen faster than we think. Nature 564 (7734), 30–32.

Yang, S., Li, S.W., Chen, B., Xie, Z.M., Peng, J., 2021. Responses of heat stress to temperature and humidity changes due to anthropogenic heating and urban expansion in South and North China. Front. Earth Sci. 9, 19. https://doi.org/10.3389/feart.2021.673943.

Yao, R., et al., 2022. Effects of urbanization on heat waves based on the wet-bulb temperature in the Yangtze River Delta urban agglomeration, China. Urban Clim. 41, 17. https://doi.org/10.1016/j.uclim.2021.101067.

Yu, L.X., Liu, Y., Liu, T.X., Yan, F.Q., 2020a. Impact of recent vegetation greening on temperature and precipitation over China. Agric. . Meteorol. 295, 11. https://doi.org/10.1016/j.agrformet.2020.108197.

Yu, Y., Zhao, W.W., Martinez-Murillo, J.F., Pereira, P., 2020b. Loess Plateau: from degradation to restoration. Sci. Total Environ. 738, 9. https://doi.org/10.1016/j.scitotenv.2020.140206.

Zander, K.K., Botzen, W.J.W., Oppermann, E., Kjellstrom, T., Garnett, S.T., 2015. Heat stress causes substantial labour productivity loss in Australia (-+). Nat. Clim. Chang. 5 (7), 647. https://doi.org/10.1038/nclimate2623.

Zhai, J., Liu, R.G., Liu, J.Y., Huang, L., Qin, Y.W., 2015. Human-induced landcover changes drive a diminution of land surface Albedo in the Loess Plateau (China. Remote Sens 7 (3), 2926–2941. https://doi.org/10.3390/rs70302926.

Zhang, G., Su, X., Hao, L., 2019. Analyzing the response of vegetation to drought based on NDVI and scPDSI from 1982 to 2015 across China. 35: 145–151. DOI:⟨10.11975/j.issn.1002–6819.2019.21.018⟩.

Zhang, M., et al., 2014. Response of surface air temperature to small-scale land clearing across latitudes. Environ. Res. Lett. 9 (3), 7. https://doi.org/10.1088/1748-9326/9/3/034002.

Zhang, X.Z., Tang, Q.H., Zheng, J.Y., Ge, Q.S., 2013. Warming/cooling effects of cropland greenness changes during 1982-2006 in the North China Plain. Environ. Res. Lett. 8 (2), 9. https://doi.org/10.1088/1748-9326/8/2/024038.

Zhang, Y.Z., Liang, S.L., 2018. Impacts of land cover transitions on surface temperature in China based on satellite observations. Environ. Res. Lett. 13 (2), 11. https://doi.org/10.1088/1748-9326/aa9e93.

Zheng, Y., et al., 2020. Effects of revegetation on climate in the Mu Us Sandy Land of China. Sci. Total Environ. 739, 13. https://doi.org/10.1016/j.scitotenv.2020.139958.

Zhu, J., Huang, D.Q., Yan, P.W., Huang, Y., Kuang, X.Y., 2017. Can reanalysis datasets describe the persistent temperature and precipitation extremes over China? Theor. Appl. Climatol. 130 (1–2), 655–671. https://doi.org/10.1007/s00704-016-1912-9.